Geosciences Journal
Vol. 20, No. 1, p. 117 − 136, February 2016
DOI 10.1007/s12303-015-0026-1

A comparative study of landslide susceptibility maps using logistic regression, frequency ratio, decision tree, weights of evidence and artificial neural network

Liang-Jie Wang* — *Jiangsu Provincial Key Laboratory of Soil Erosion and Ecological Restoration, Nanjing Forestry University, Nanjing 210037, China*; *College of Forestry, Nanjing Forestry University, Nanjing 210037, China*
Min Guo, Kazuhide Sawada — *Graduate School of Engineering, Gifu University, Gifu 5011193, Japan*
Jie Lin, Jinchi Zhang — *College of Forestry, Nanjing Forestry University, Nanjing 210037, China*

ABSTRACT: For the purpose of comparing susceptibility mapping methods in Mizunami City, Japan, the landslide inventory was partitioned into three groups as various training and test datasets to identify the most appropriate method for creating a landslide susceptibility map. A total of fifteen landslide susceptibility maps were produced using frequency ratio, logistic regression, decision tree, weights of evidence and artificial neural network models, and the results were assessed using existing test landside points and areas under the relative operative characteristic curve (AUC). The validation results indicated that the logistic regression model could provide the highest AUC value (0.865), and a relatively high percentage of landslide points fell in the high and very high landslide susceptibility classes in this study. Furthermore, the paper also suggested that the model performances would be increased if appropriate landslide points were used for the calculation.

Key words: landslide susceptibility mapping, logistic regression (LR), frequency ratio (FR), decision tree (DT), weights of evidence (WOE), artificial neural network (ANN)

1. INTRODUCTION

Landslides are considered to be the most common geological disaster, causing loss of human life and damage to the economy (Bui et al., 2012; Shahabi et al., 2014). In the published research literature, three main methodologies for assessing landslide susceptibility and hazards were proposed: heuristic, deterministic and quantitative. During the last decade, the implementation of quantitative methods in geographic information systems (GIS) was widely applied for landslide susceptibility analysis. Several different quantitative approaches to evaluate the landslide susceptibility can be found in the current literature, including frequency ratio (Yalcin et al., 2011; Ozdemir and Altural, 2013), logistic regression analysis (Bai et al., 2010; Das et al., 2010; Pradhan, 2010a, 2010b; Wang et al., 2013; Althuwaynee et al., 2014; Shahabi et al., 2014), bivariate statistic analysis (Nandi and Shakoor, 2010; Xu et al., 2012), weights of evidence (Regmi et al., 2010a, 2010b), artificial neural networks (Poudyal et al., 2010; Pradhan et al., 2010; Yilmaz, 2010; Bui et al., 2012; Conforti et al., 2014), and decision trees (Saito et al., 2009; Yeon et al., 2010; Althuwaynee et al., 2014).

In recent years, some studies have compared landslide susceptibility maps by using these quantitative methods. Yilmaz (2010), Pradhan and Lee (2010a, 2010b) compared the landslide susceptibility (LS) maps by using the frequency ratio (FR), logistic regression (LR) and artificial neural network (ANN) models, whereas Ozdemir and Altural (2013) presented a comparative study of FR, LR and weights of evidence (WOE) models for landslide susceptibility analysis. Xu et al. (2012) compared LR with bivariate statistics (BS) and ANN, and found LR to be the most efficient of these techniques. Pradhan (2013) assessed the predictive ability of a decision tree (DT) model with two other mathematical models. Moreover, a new landslide susceptibility analysis method, multivariate adaptive regression splines (MARSplines) proposed by Felicisimo et al. (2013), was adopted to compare the landslide susceptibility maps with DT and LR. Despite the popularity of the above methods, few studies have been carried out on landslide susceptibility analysis using FR, LR, WOE, ANN, and DT applied separately for landslide susceptibility mapping in different areas. In this study, the five mathematical models have been applied to analyze landslide susceptibility for the first time in Mizunami City, Gifu Prefecture, Japan. The results obtained from these models with different training datasets are compared to determine the most suitable method for landslide susceptibility mapping. The effective LS maps will help the local government implement city planning, infrastructure construction, and agricultural development schemes.

2. STUDY AREA

The Mizunami City is located in the southeastern region of Gifu Prefecture, Japan, which covers an area of 175 km^2 (Fig. 1). The elevation in this area ranges from 137 m to 792

*Corresponding author: pawangwlj@outlook.com

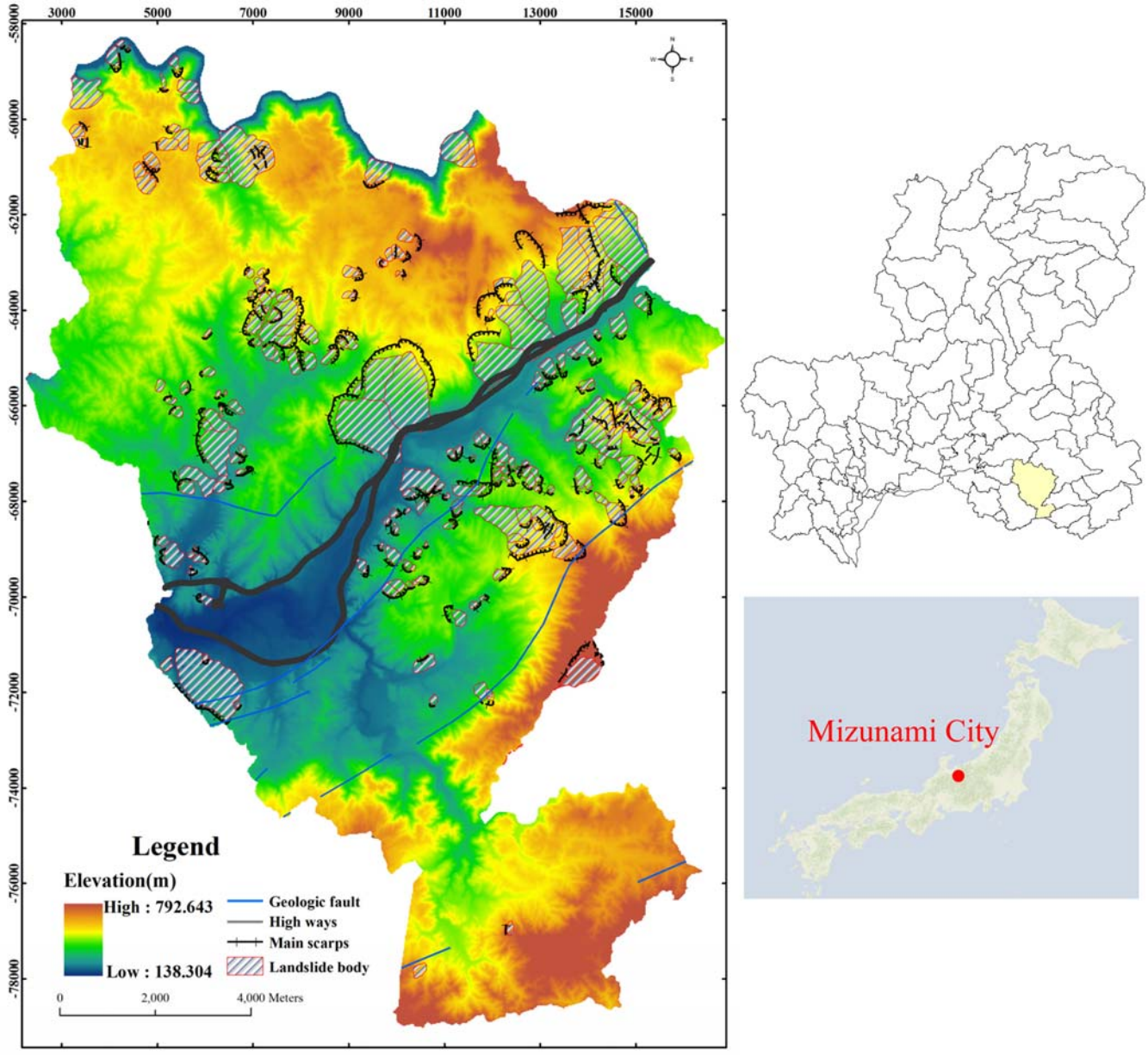

Fig. 1. Geographical location of Mizunami City, Gifu Prefecture, Japan.

m, and steep slopes are very common. The monthly precipitation ranges from 47.7 mm to 263.1 mm (Japan Meteorological Agency). Typhoons occasionally bring intense precipitation and cause landslides and debris flows in the city. In the study area, based on the landslide classification system of Varnes (1978), the predominant type of landslide is translational slides, which has appeared on cut slopes or embankments along two highways, Chuo Expressway and Japan National Route 21. The geological components of the study area are primarily sedimentary rocks, plutonic rocks, volcanic rocks, granite and sandstone. Generally speaking, intense or prolonged rainfall, snow melting and human activity substantially influence the slopes in the study area.

3. SPATIAL DATABASE PREPARATION

3.1. Landslide Inventory Map

The preparation of a landslide inventory map is the first step of LS analysis. A landslide inventory map records the locations, characteristics, and outlines of landslides (Ozdemir and Altural, 2013). In the study area, the inventory map including scarp areas and landslide bodies was provided by NIED (National Research Institute for Earth Science and Disaster Prevention, http://www.bosai.go.jp/activity_special/data; http://lsweb1.ess.bosai.go.jp). The numbers of the landslide bodies are 219. The size of landslide body ranges from 2.5 ×

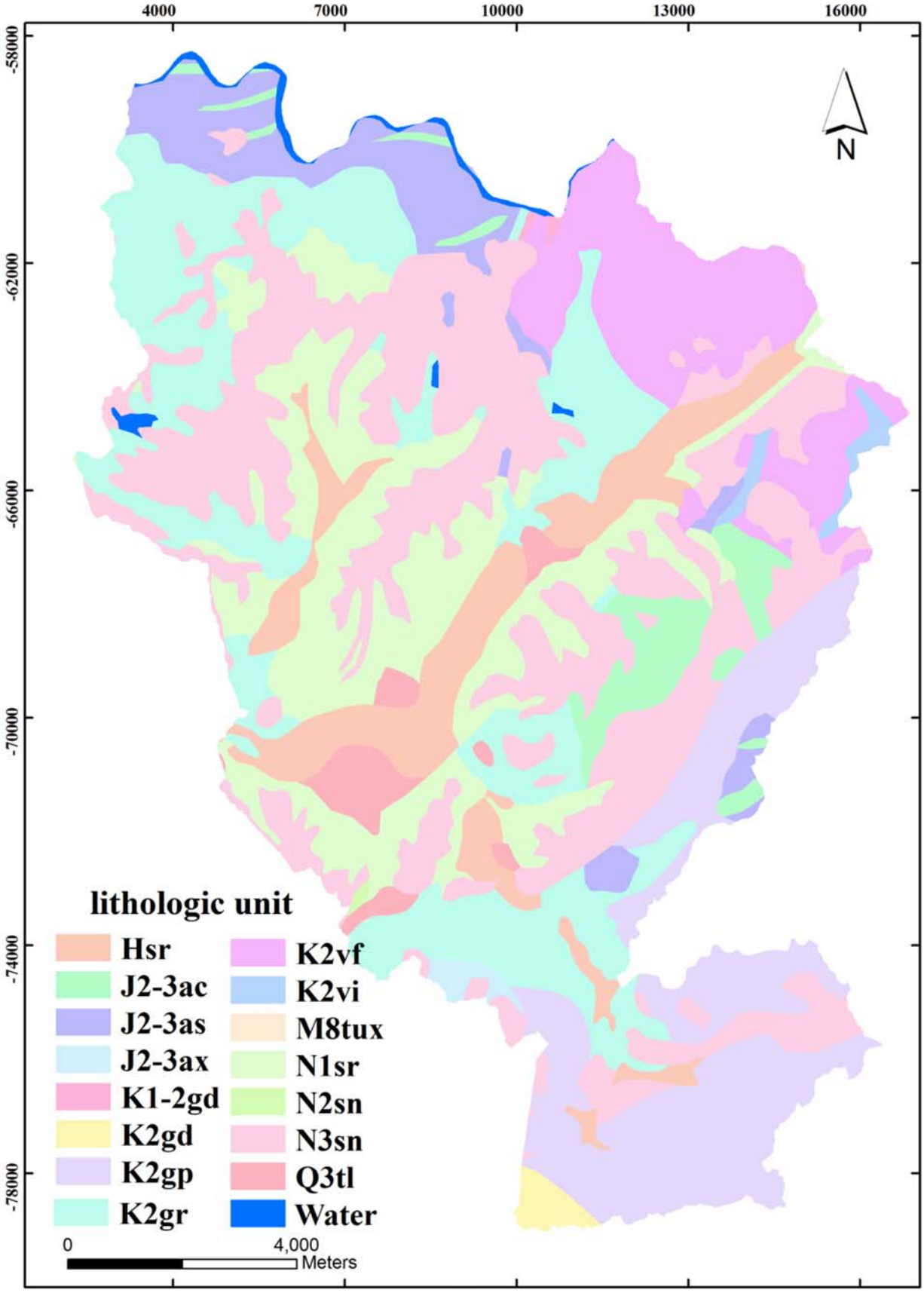

Fig. 2. Geology condition map of Mizunami City.

10^{-3} km^2 to 1.25 km^2. Previous studies had revealed that the landslide area percentage (LAP) and the landslide number density (LND) are 12.9% and 1.26 landslides/ km^2, respectively (Wang et al., 2013). Detailed information about LAP and LND can be found in the literature (Xu et al., 2012).

3.2. Landslide Conditioning Factor

Collecting ideal landslide conditioning factors at a suitable scale is an intriguing task (Pradhan, 2013) that requires comprehensive knowledge to understand the conditioning factors and to recognize the importance of each factor. In this study, a topographic dataset, a water-related dataset, a geological/land cover dataset, and a human activities dataset were constructed for LS analyses. The critical point was the selection of appropriate pixel size for positional accuracy and precision of susceptibility levels in the resultant map (Shahabi et al., 2014). Wang et al. (2013) showed that a pixel size of 10 m was enough for LS analysis in the study area. A digital elevation model (DEM) is built by using LiDAR (Airborne Light Detection and Ranging) points and a triangulated irregular network (TIN), and then converted to a 10 m raster-based data layer using GIS software.

The topographic parameters elevation, slope angle, and curvature were derived from the digital elevation model (DEM). Slope is viewed as the major conditioning factor, which is frequently used in the calculation of landslide susceptibility analysis (Nandi and Shakoor, 2010; Xu et al., 2012; Yalcin et al., 2011; Wang et al., 2013; Shahabi et al., 2014). According to the importance of slope conditions and configurations in landslide occurrence, the study area was divided into ten slope categories as (0–5°), (5–10°), (10–15°), (15–20°), (20–25°), (25–30°), (30–35°), (35–40°), (40–45°) and (>45°), which are shown in Table 2. Elevation is also considered as an important factor in landslide susceptibility mapping (Xu et al., 2012). According to the obtained map of the DEM, the elevation of the study area was classified into ten classes using 50 m intervals: (<150), (150–200), (200–250), (250–300), (300–350), (350–400), (400–450), (450–500), (500–550) and (>550) m. For the classification of the curvature, the grid map of the parameter was obtained from the DEM. The curvature of the study area was classified into ten classes using 0.5 intervals: (<–1.5), (–1.5 – (–1)), ((–1) – (–0.5)), (–0.5 – 0), (0–0.5), (0.5–1), (1–1.5), (1.5–2), (2–2.5) and (>2.5).

The water-related dataset, including flow direction, topographic wetness index (TWI) and the distance-to-streams factor, was derived from the DEMs and river distribution maps. The flow direction derived from DEM was classified into 8 directions: (1 (E)), (2 (SE)), (4 (S)), (8 (SW), (16 (W)), (32 (NW), (64 (N) and (128 (NE). The closeness of the slope to a stream is another important factor in terms of stability. Streams may adversely affect stability by eroding the slope or by saturating the lower part of the material, possibly resulting in an increase in the height of the water table at the base of the slope (Yalcin, 2008; Nourani et al., 2014). In the case of the map of the distance to the stream, ten classes were made using the buffer tool in ArcGIS software with 200 m intervals: (<200), (200–400), (400–600), (600–800), (800–1000), (1000–1200), (1200–1400), (1400–1600), (1600–1800) and (>1800) m. Regardless of the sampling strategy, most landslides are observed to occur near the stream (0–400 m). In the TWI (–3 – 3) map, which was derived from the DEM, ten categories were created for the analysis. For the classification of the flow direction, the grid map of the parameters was obtained from the DEM.

Landslides may occur on roads and on the side of the slopes affected by roads (Yalcin, 2008). According to recent studies, cutting slopes for highway construction and frequency vibrations caused by cars could induce landslides (Mittal et

Table 1. lithologies of the geological unit in the study area

Geologic unit	Description
Hsr	Late Pleistocene to Holocene marine and non-marine sediments
J2-3as	Sandstone of Middle to Late Jurassic accretionary complex
J2-3ac	Triassic to Middle Jurassic chert block of Middle to Late Jurassic accretionary complex
J2-3ax	Melange matrix of Middle to Late Jurassic accretionary complex
K1-2gd	Early to Late Cretaceous granodiorite (Older Ryoke Granite)
K2gp	Late Cretaceous felsic plutonic rocks (Younger Ryoke Granite)
K2gr	Late Cretaceous granite (Younger Ryoke Granite)
K2gd	Late Cretaceous granodiorite (Younger Ryoke Granite)
K2vf	Late Cretaceous non-alkaline felsic volcanic rocks
K2vi	Late Cretaceous non-alkaline felsic volcanic intrusive rocks
M8tux	Ryoke Metamorphic rocks (gneiss and schist)
N1sr	Early Miocene to Middle Miocene marine and non-marine sediments
N2sn	Middle to Late Miocene non-marine sediment
N3sn	Late Miocene to Pliocene non-marine sediments
Q3tl	Late Pleistocene lower terrace

Table 2. landslide conditioning factors in the analyses and results from the frequency ration and weights of evidence approaches

Mathematical	Methods			FR			WOE			WOE			WOE	
Factors	Sampling		RD	TD	RL		RD			TD			RL	
	class	id				W–	W+	W_c	W–	W+	W_c	W–	W+	W_c
Elevation	≤150	1	0.0	0.0	0.0	0.0	0.0	0.0	0.0	0.0	0.0	0.0	0.0	0.0
(m)	150–200	2	0.3	0.1	0.1	0.1	–1.1	–1.2	0.1	–2.2	–2.3	0.1	–2.2	–2.2
	200–250	3	1.2	0.8	0.9	–0.0	0.2	0.2	0.0	–0.3	–0.3	0.0	–0.1	–0.2
	250–300	4	1.6	1.7	1.5	–0.1	0.5	0.5	–0.1	0.5	0.6	–0.1	0.4	0.4
	300–350	5	1.6	1.7	1.6	–0.1	0.5	0.6	–0.1	0.6	0.7	–0.1	0.5	0.6
	350–400	6	1.3	1.3	1.5	–0.1	0.2	0.3	–0.1	0.3	0.4	–0.1	0.4	0.6
	400–450	7	0.8	0.9	0.9	0.0	–0.2	–0.2	0.0	–0.1	–0.1	0.0	–0.1	–0.1
	450–500	8	0.5	0.7	0.4	0.1	–0.7	–0.7	0.0	–0.4	–0.4	0.1	–0.9	–1.0
	500–550	9	0.1	0.1	0.2	0.1	–2.2	–2.2	0.1	–2.1	–2.1	0.1	–1.8	–1.8
	>550	10	0.3	0.0	0.5	0.0	–1.2	–1.2	0.0	0.0	0.0	0.0	–0.7	–0.7
Slope angle	0–5	1	0.4	0.4	0.5	0.1	–0.9	–1.0	0.1	–0.9	–0.9	0.1	–0.8	–0.9
(degree)	5–10	2	1.0	1.1	1.1	–0.0	0.0	0.0	–0.0	0.1	0.1	–0.0	0.1	0.1
	10–15	3	1.3	1.3	1.3	–0.1	0.2	0.3	–0.1	0.3	0.4	–0.1	0.3	0.4
	15–20	4	1.2	1.1	1.2	–0.0	0.2	0.2	–0.0	0.1	0.1	–0.0	0.2	0.2
	20–25	5	1.0	0.9	1.0	–0.0	0.0	0.0	0.0	–0.1	–0.1	0.0	–0.0	–0.0
	25–30	6	1.0	0.8	0.8	0.0	–0.0	–0.0	0.0	–0.2	–0.2	0.0	–0.2	–0.2
	30–35	7	0.9	0.8	0.7	0.0	–0.2	–0.2	0.0	–0.2	–0.2	0.0	–0.3	–0.3
	35–40	8	0.9	0.9	0.9	0.0	–0.1	–0.1	0.0	–0.1	–0.1	0.0	–0.2	–0.2
	40–45	9	1.1	1.2	1.0	–0.0	0.1	0.1	–0.0	0.2	0.2	0.0	–0.0	–0.0
	>45	10	1.1	1.4	1.2	–0.0	0.1	0.1	–0.0	0.3	0.3	–0.0	0.2	0.2
				FR		W–	W+	W_c	W–	W+	W_c	W–	W+	W_c
Distance to	≤200	1	0.9	0.4	0.9	0.0	–0.1	–0.1	0.0	–0.8	–0.9	0.0	–0.1	–0.1
faults (m)	200–400	2	0.8	0.4	0.9	0.0	–0.2	–0.2	0.0	–0.9	–0.9	0.0	–0.1	–0.1
	400–600	3	0.7	0.5	0.7	0.0	–0.3	–0.3	0.0	–0.6	–0.7	0.0	–0.3	–0.3
	60–800	4	0.9	0.7	1.1	0.0	–0.1	–0.1	0.0	–0.3	–0.3	–0.0	0.1	0.1
	800–1200	5	1.3	1.0	1.6	–0.1	0.3	0.3	–0.0	0.0	0.0	–0.1	0.4	0.5
	1200–1600	6	1.5	1.2	2.1	–0.1	0.4	0.5	–0.0	0.2	0.2	–0.2	0.7	0.9
	1600–2000	7	1.2	1.5	1.6	–0.0	0.2	0.2	–0.1	0.4	0.5	–0.1	0.5	0.5
	2000–3000	8	0.7	1.1	0.5	0.0	-0.3	–0.4	–0.0	0.1	0.1	0.1	–0.6	–0.7
	3000–5000	9	0.6	0.9	0.5	0.1	–0.5	–0.6	0.0	–0.1	–0.1	0.1	–0.8	–0.9
	>5000	10	1.0	1.5	0.0	0.0	–0.0	–0.0	–0.1	0.4	0.5	0.1	–4.1	–4.2
Land use	water	0	0.0	0.0	0.0	0.0	0.0	0.0	0.0	0.0	0.0	0.0	0.0	0.0
	Residential	1	0.7	0.9	0.7	0.0	–0.4	–0.4	0.0	–0.1	–0.2	0.0	–0.3	–0.3
	Bamboo	2	4.8	6.4	0.0	–0.0	1.6	1.6	–0.0	1.9	1.9	0.0	0.0	0.0
	Cropland	3	0.7	0.9	0.5	0.0	–0.4	–0.5	0.0	–0.1	–0.1	0.1	–0.7	–0.8
	Forest	4	0.7	0.6	0.4	0.1	–0.4	–0.5	0.1	–0.5	–0.7	0.2	–1.0	–1.2
	Grassland	5	1.5	0.7	2.3	–0.0	0.4	0.4	0.0	–0.4	–0.4	–0.1	0.9	0.9
	Herbaceous	6	0.7	0.3	0.8	0.0	–0.4	–0.4	0.0	–1.1	–1.1	0.0	–0.2	–0.2
	Plantation	7	1.2	0.9	1.1	–0.0	0.2	0.2	0.0	–0.1	–0.2	–0.0	0.1	0.2
	Woodland	8	1.4	1.8	1.7	–0.2	0.4	0.5	–0.3	0.6	0.9	–0.2	0.5	0.8
Distance to	≤200	1	1.2	1.3	1.3	–0.1	0.2	0.2	–0.1	0.2	0.4	–0.1	0.3	0.4
Streams (m)	200–400	2	1.2	1.3	1.2	–0.1	0.2	0.3	–0.1	0.2	0.3	–0.1	0.2	0.3
	400–600	3	1.0	1.1	0.9	–0.0	0.0	0.0	–0.0	0.1	0.1	0.0	–0.1	–0.1
	600–800	4	1.0	0.8	0.9	0.0	–0.0	–0.0	0.0	–0.2	–0.3	0.0	–0.1	–0.1

Table 2. (continued)

				FR		W–	W+	W_c	W–	W+	W_c	W–	W+	W_c
	800–1000	5	0.8	0.6	0.6	0.0	–0.2	–0.3	0.0	–0.5	–0.5	0.0	–0.5	–0.5
	1000–1200	6	0.4	0.4	0.2	0.0	–0.9	–0.9	0.0	–0.9	–0.9	0.0	–1.6	–1.6
	1200–1400	7	0.2	0.3	0.0	0.0	–1.7	–1.7	0.0	–1.3	–1.3	0.0	–5.0	–5.0
	1400–1600	8	0.3	0.2	0.3	0.0	–1.1	–1.1	0.0	–1.6	–1.6	0.0	–1.2	–1.2
	1600–1800	9	0.4	0.0	0.7	0.0	–0.9	–0.9	0.0	0.0	0.0	0.0	–0.4	–0.4
	>1800	10	0.5	0.0	0.7	0.0	–0.8	–0.8	0.0	0.0	0.0	0.0	–0.3	–0.3
TWI	≤–1	1	0.7	0.6	0.5	0.0	–0.4	–0.4	0.0	–0.5	–0.5	0.0	–0.7	–0.8
	–1 – (–0.5)	2	0.9	0.8	0.8	0.0	–0.1	–0.1	0.0	–0.2	–0.2	0.0	–0.3	–0.3
	–0.5 – 0	3	1.0	1.0	0.9	–0.0	0.0	0.0	–0.0	0.0	0.0	0.0	–0.1	–0.1
	0–0.5	4	1.1	1.1	1.0	–0.0	0.1	0.1	–0.0	0.1	0.1	–0.0	0.0	0.1
	0.5-1	5	1.2	1.2	1.2	–0.0	0.2	0.2	–0.0	0.2	0.2	–0.0	0.2	0.2
	1–1.5	6	1.2	1.2	1.3	–0.0	0.2	0.3	–0.0	0.2	0.2	–0.0	0.3	0.3
	1.5–2	7	1.1	1.3	1.3	–0.0	0.1	0.1	–0.0	0.2	0.3	–0.0	0.3	0.3
	2–2.5	8	1.0	1.1	1.1	0.0	–0.0	–0.0	–0.0	0.1	0.1	–0.0	0.1	0.1
	2.5–3	9	0.7	0.8	0.9	0.0	–0.3	–0.3	0.0	–0.3	–0.3	0.0	–0.1	–0.1
	>3	10	0.2	0.3	0.3	0.1	–1.4	–1.4	0.0	–1.2	–1.3	0.0	–1.1	–1.1
Flow direction	1(E)	1	1.1	1.3	1.1	–0.0	0.1	0.1	–0.0	0.3	0.3	–0.0	0.1	0.1
	2(SE)	2	1.3	1.7	1.4	–0.0	0.3	0.3	–0.1	0.5	0.6	–0.0	0.3	0.4
	4(S)	3	1.2	1.4	1.2	–0.0	0.2	0.2	–0.1	0.3	0.4	–0.0	0.2	0.2
	8(SW)	4	1.0	1.1	1.0	0.0	–0.0	–0.0	–0.0	0.1	0.1	0.0	–0.0	–0.0
	16(W)	5	0.8	0.7	0.8	0.0	–0.2	–0.2	0.1	–0.4	–0.4	0.0	–0.2	–0.2
	32(NW)	6	0.8	0.5	0.8	0.0	–0.2	–0.2	0.1	–0.6	–0.7	0.0	–0.2	–0.2
	64(N)	7	0.8	0.5	0.8	0.0	–0.2	–0.2	0.1	–0.7	–0.7	0.0	–0.2	–0.2
	128(NE)	8	1.0	1.0	1.0	–0.0	0.0	0.1	0.0	–0.0	–0.0	–0.0	0.0	0.0
				FR		W–	W+	W_c	W–	W+	W_c	W–	W+	W_c
Distance to highways (m)	≤500	1	1.5	1.9	2.2	–0.1	0.4	0.5	–0.1	0.6	0.8	–0.2	0.8	0.9
	500–1000	2	2.2	2.1	2.3	–0.1	0.8	0.9	–0.1	0.8	0.9	–0.1	0.9	1.0
	1000–1500	3	1.8	1.9	2.0	–0.1	0.6	0.6	–0.1	0.6	0.7	–0.1	0.7	0.8
	1500–2000	4	0.8	0.3	1.2	0.0	–0.2	–0.2	0.1	–1.2	–1.2	–0.0	0.2	0.2
	2000–3000	5	1.1	0.6	1.2	–0.0	0.1	0.1	0.1	–0.5	–0.6	–0.0	0.2	0.2
	3000–4000	6	0.8	0.8	0.6	0.0	–0.2	–0.2	0.0	–0.2	–0.2	0.1	–0.6	–0.6
	4000–5000	7	0.4	0.5	0.4	0.1	–1.0	–1.0	0.1	–0.6	–0.7	0.1	–0.9	–0.9
	5000–6000	8	0.2	0.0	0.2	0.1	–1.7	–1.8	0.1	–3.3	–3.3	0.1	–1.4	–1.5
	6000–8000	9	0.6	0.9	0.1	0.1	–0.5	–0.5	0.0	–0.1	–0.1	0.1	–3.0	–3.1
	>8000	10	0.5	0.8	0.0	0.0	–0.7	–0.7	0.0	–0.2	–0.3	0.0	0.0	0.0
Curve	≤–1.5	1	0.5	0.5	0.5	0.1	–0.6	–0.7	0.1	–0.7	–0.8	0.1	–0.8	–0.9
	–1.5 – (–1)	2	1.5	1.6	1.5	–0.0	0.4	0.5	–0.0	0.5	0.5	–0.0	0.4	0.4
	–1 – (–0.5)	3	1.2	1.3	1.3	–0.0	0.2	0.2	–0.0	0.3	0.3	–0.0	0.2	0.3
	–0.5 – 0	4	1.0	1.0	1.1	0.0	–0.0	–0.0	–0.0	0.0	0.0	–0.0	0.1	0.1
	0–0.5	5	1.1	1.1	1.1	–0.0	0.1	0.1	–0.0	0.1	0.1	–0.0	0.1	0.2
	0.5–1	6	1.3	1.3	1.3	–0.0	0.3	0.3	–0.0	0.2	0.3	–0.0	0.2	0.3
	1–1.5	7	1.3	1.2	1.2	–0.0	0.2	0.3	–0.0	0.2	0.2	–0.0	0.2	0.2
	1.5–2	8	1.2	1.2	1.1	–0.0	0.2	0.2	–0.0	0.2	0.2	–0.0	0.1	0.1
	2–2.5	9	1.5	1.4	1.3	–0.0	0.4	0.4	–0.0	0.3	0.3	–0.0	0.3	0.3
	>2.5	10	0.4	0.4	0.3	0.1	–0.9	–1.0	0.1	–1.0	–1.1	0.1	–1.1	–1.2

Table 2. (continued)

Geologic				FR		W–	W+	W_c	W–	W+	W_c	W–	W+	W_c
	Hsr	1	0.8	1.2	1.1	0.0	–0.2	–0.2	–0.0	0.2	0.2	–0.0	0.1	0.1
	J2-3ac	2	2.3	0.2	3.6	–0.0	0.8	0.9	0.0	–1.5	–1.6	–0.1	1.3	1.4
	J2-3as	3	1.1	1.5	0.4	–0.0	0.1	0.1	–0.0	0.4	0.5	0.0	–1.0	–1.0
	J2-3ax	4	0.0	0.0	0.0	0.0	0.0	0.0	0.0	0.0	0.0	0.0	0.0	0.0
	K1-2gd	5	0.0	0.0	0.0	0.0	0.0	0.0	0.0	0.0	0.0	0.0	0.0	0.0
	K2gd	6	0.0	0.0	0.0	0.0	0.0	0.0	0.0	0.0	0.0	0.0	0.0	0.0
	K2gp	7	0.1	0.0	0.1	0.1	–2.7	–2.8	0.0	0.0	0.0	0.1	–2.2	–2.3
	K2gr	8	0.9	1.2	0.5	0.0	–0.1	–0.1	–0.0	0.2	0.2	0.1	–0.7	–0.8
	K2vf	9	2.4	3.2	3.9	–0.1	0.9	1.0	–0.2	1.2	1.4	–0.3	1.4	1.7
	K2vi	10	1.4	0.0	2.3	–0.0	0.3	0.3	0.0	0.0	0.0	–0.0	0.8	0.8
	M8tux	11	0.0	0.0	0.0	0.0	0.0	0.0	0.0	0.0	0.0	0.0	0.0	0.0
	N1sr	12	1.1	0.9	0.6	–0.0	0.1	0.1	0.0	–0.1	–0.2	0.1	–0.5	–0.5
	N2sn	13	0.0	0.0	0.0	0.0	0.0	0.0	0.0	0.0	0.0	0.0	0.0	0.0
	N3sn	14	1.0	0.8	0.9	0.0	–0.0	–0.1	0.1	–0.3	–0.4	0.0	–0.1	–0.2

al., 2008; Regmi et al., 2010a). The distance to two major highways, the Chuo expressway and Japan National Route 21, are calculated using GIS. For designating the influence of the highways on the slope stability, the study area was divided into ten different buffer categorizes: (<500), (500–1000), (1000–1500), (1500–2000), (2000–3000), (3000–4000), (4000–5000), (5000–6000), (6000–8000) and (>8000) m. Most landslides occur near the road (0–1500 m) with different sampling strategies, but the extended area of this class is large. There are plenty of landslide pixels that fell into other buffer categories. In this study, only two major highways have been considered.

The geological map and distances to faults used to represent the features of the slope materials and the co-seismic conditions were provided by the Geological Survey of Japan, AIST. Note that the geology of our study area is very complex and the lithologic units comprise several formations (Fig. 2). The formations were therefore classified into fifteen categories with respect to landslide susceptibility. The descriptions of the geological units are provided in Table 1. Geological faults are an important susceptibility factor. For designating the influence of the faults on slope stability, the study area was divided into ten different buffer categorizes: (<200), (200–400), (400–600), (600–800), (800–1200), (1200–1600), (1600–2000), (2000–3000), (3000–5000) and (>5000) m as shown as Table 2.

The land cover map is also a factor for predicting landslide occurrence. All of the landslide conditioning factors from the above datasets were stored in the spatial database using a spatial analysis tool (ArcGIS software) with a spatial resolution of 10 m.

4. LANDSLIDE SUSCEPTIBILITY MAPPING

4.1. Training and Testing Datasets

The way we choose the training dataset may affect landslide susceptibility mapping results. Vahidnia et al. (2010) and Yeon et al. (2010) used partial landslide points to denote the training dataset, and used a subset of these points for the testing dataset. Nandi and Shakoor (2010) partitioned the landslide inventory into two subsets: landslides in the left part of the study area were used as the training dataset, and those of the right part were used as the testing dataset. Pradhan (2013) used 50% of landslide grid cells for training, and other 50% for testing were selected at random. In this study, the landslide inventory was divided into three different subsets including: (1) half of the landslide points for training by random selection, and half for testing (abbreviation as RD sampling strategy); (2) landslide points from the right side of dividing line 1 for training, and the left side for testing (abbr. RL sampling strategy); (3) landslide points from above line 2 for training, and below for testing (abbr. TD sampling strategy) (Fig. 3). For the BS model, only the landslide data are required. However, it is necessary to obtain satisfactory sample data representing the absence of landslide occurrence to fit the LR and ANN models (Xu et al., 2012). For the RD sampling strategies, the numbers of landslide free points from the region of stable slopes in the study area were chosen randomly to be the same as the selected landslide points. For testing data, we use the remaining half of the grid cells of the landslide points and non-landslide points. For the RL and TD sampling approaches, the non-landslide points were selected randomly from the training area, divided by lines 1 and 2, and the testing datasets were chosen from the testing area. Additionally, the ratio of landslide points to non-landslide points is equal to 1.

4.2. Frequency Ratio Model (FR)

The frequency ratio (FR) model is a simple tool to calculate the probabilistic relationship between a landslide and landslide conditional factors (Ozdemir and Altural, 2013). The FR is the ratio of the area where landslides have occurred to the

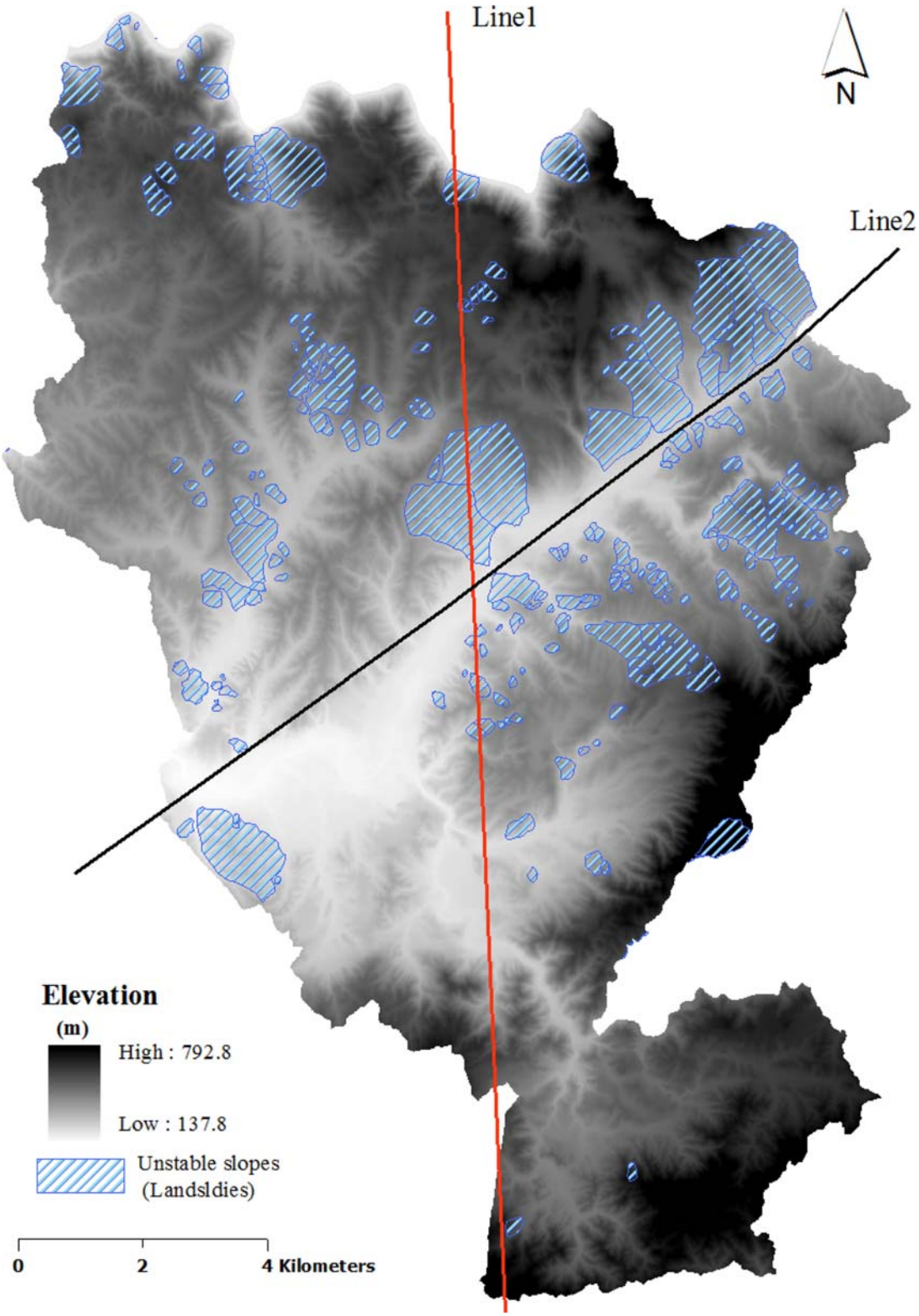

Fig. 3. Landslide inventory map of Mizunami City with dividing lines of the training and test areas.

total study area and is also the ratio of the landslide occurrence probability to the non-occurrence probability for a given attribute (Lee and Talib, 2005). First, the frequency ratio of each range or type of factor is calculated, then the FRs are summed with Equations (1) and (2) as the landslide susceptibility index (LSI) (Yilmaz, 2010).

$$FR = \frac{D_i / \sum_{i=1}^{N} D_i}{A_i / \sum_{i=1}^{N} A_i}, \quad (1)$$

$$\mathrm{LSI} = \sum FR, \quad (2)$$

where D_i is the area of landslide of the i-th category, A_i is the area of the i-th category for a certain parameter and N is the category number of the parameter. The results obtained by the FR method are easy to understand. A FR value greater than 1 indicates a high probability of landslide occurrence, and a value less than 1 indicates a low correlation (Oh et al., 2010; Ozdemir and Altural, 2013). The FR values of the conditioning factors are reported in Table 2. Although the training datasets are different, the FR of the relationship between LSI and land use/cover is higher in woodland areas than in other land use areas, except for the bamboo area. The bamboo area has the highest FR value except when choosing the RL sampling strategy. The FR values for the relationship between LSI and geology are higher in J2-3ac and K2vf. However, the FR value of J2-3ac indicates a low correlation using the TD sampling points because only a small percentage of landslide points fell in the J2-3ac class using the TD sampling strategy according to Figure 3 and Table 2. Relationships between curvature and landslide occurrence indicate that landslides generally do not occur near areas with curvature values smaller than –1.5 or larger than 2.5. Flow directions with E, SE, and S directions have stronger relationships than other areas and exhibit high probabilities of LS. FR values are larger where TWI ranges from 0.5–2, which indicates a high correlation. The FR analyses demonstrate that the areas with slopes between 10–20° have high probabilities of landslide occurrence. There are no significant differences between slope classes, because in Japan, the potential landslides do not have steep slopes as in USA and China (Wang et al., 2013). LS is also high in the areas where the elevations range from 250–400 m; when the elevations are higher than 400 m or lower than 250 m, the probabilities of LS decrease. The distance to streams smaller than 400 m has a stronger relationship with LS than other factors, and areas with small distances to streams have high probabilities of LS. Relationships between distance to highways and landslide occurrence indicate that landslides generally occurred near the highways, with distances smaller than 1500 m. A distance of 1500 m from a highway may not induce landslide occurrence, but there is a significant correlation between the extent and frequency of landslides on one hand and distance to the regional highways system on the other (Shahabi et al., 2014). In the study area, the highway system causes cuts to form in slopes, thereby destabilizing them.

Thus the contrast value is higher for distances to highways less than 1500 m compared with other classes, as there are plenty of pixels compared to other classes. However, the spatial relationship between landslide occurrence and highway construction is very close, especially in the study area. The ratio between LS and distance to faults is larger than 1 for distance to faults values between 800 m and 2000 m, revealing a high correlation with LS. From Table 2, there is a possibility that geological factors influence landslide occurrence rather than distance to faults. The LS maps produced from the FR model are given in Figure 4.

4.3. Weights of Evidence Model (WOE)

WOE is a Bayesian approach in a log-linear form, which

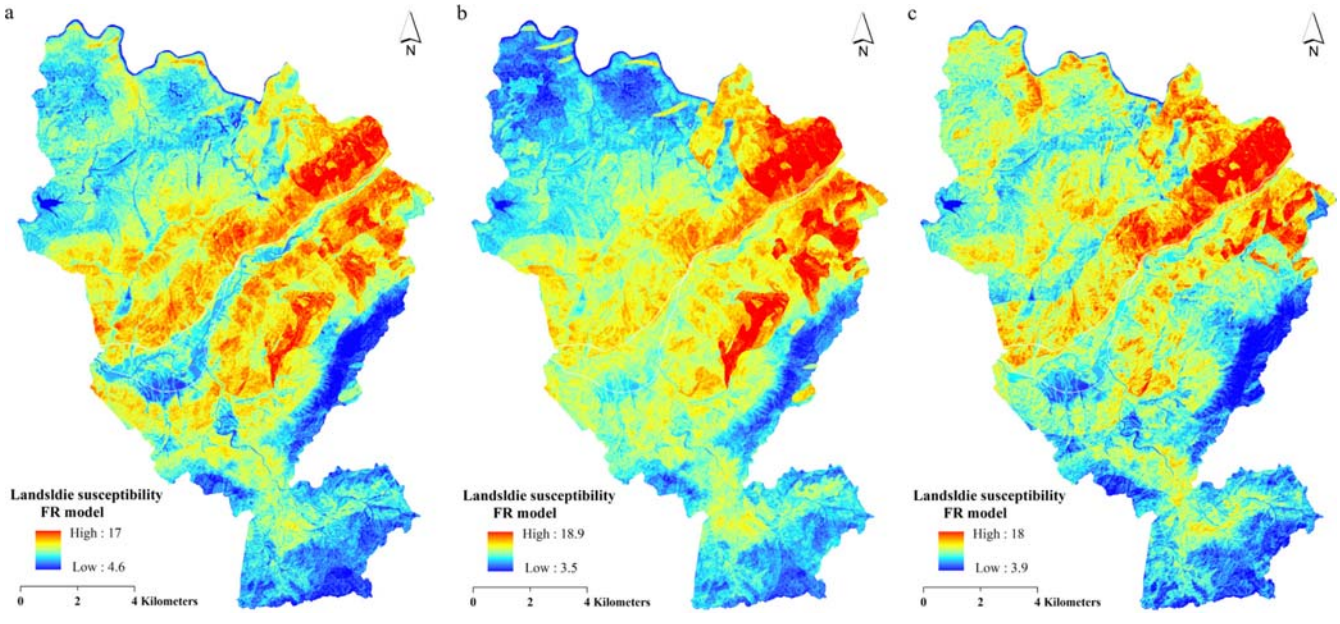

Fig. 4. landslide susceptibility maps using FR model. (a) RD sampling strategy; (b) RL sampling strategy; (c) TD sampling strategy.

uses prior probability and posterior probability (Regmi et al., 2010a). The detailed theoretical background and algorithm of WOE can be found in Regmi et al. (2010a, 2010b). The WOE approach has been widely applied in many studies (Van Westan et al., 2003; Regmi et al., 2010a, 2010b; Neuhauser et al., 2011; Ozdemir and Altural, 2013). Weight values for the classes of landslide conditioning factors are calculated by the following equations (Regmi et al., 2010a):

$$W^{+} = \ln\left[\frac{\frac{A1}{A1+A2}}{\frac{A3}{A3+A4}}\right], \quad (3)$$

$$W^{-} = \ln\left[\frac{\frac{A2}{A1+A2}}{\frac{A4}{A3+A4}}\right], \quad (4)$$

where A1 is the number of landslide pixels present in a given factor class. A2 is the number of landslide pixels not present in the same given factor class. A3 is the number of pixels in a given class in which no landslide pixels are present, and A4 is the number of pixels in the given factor class when neither landslide nor the given factor is present (Regmi et al., 2010a, 2010b; Ozdemir and Altural, 2013).

Positive and negative weights (W^+ and W^-) reveal the relationship between the conditioning factors and landslides. A positive weight indicates the presence of a conditioning factor for landslides, and the magnitude of the weight shows the positive correlation between the presence of a conditioning factor and a landslide. In contrast, the negative weight indicates an absence of a conditioning factor, and the magnitude indicates a negative correlation (Regmi et al., 2010a; Ozdemir and Altural, 2013). The W_c ($W_c = W^+ - W^-$) value, which is defined as the difference between W^+ and W^-, reflects the overall spatial association between a conditioning factor and a landslide occurrence (Regmi et al., 2010a; Xu et al., 2012). A positive W_c value indicates a positive spatial correlation between a conditioning factor and a landslide, whereas a negative W_c value indicates unfavorable conditions for a landslide (Regmi et al., 2010a, 2010b; Ozdemir and Altural, 2013). A weigh contrast close to zero indicates that the factor is not significant for analyzing a landslide. The final probability (P) of each cell is the sum of the weights of each parameter and the prior probability $P_p(S)$ (Ozdemir and Altural, 2013). The final probability is calculated by employing the following equations

$$P = \exp\{\sum W^{+} + \ln P_p(S)\}, \quad (5)$$

$$P_p(S) = \frac{N_L}{N_P}, \quad (6)$$

where N_L is the number of landslide pixels, and N_p is the total number of study area pixels.

For each of the landslide conditioning factors, the weights, contrasts, and probability values were calculated using different training datasets with Equations (3)–(6) as shown in Table 2. The conditioning independence of the factors was tested using chi-square statistics. The results suggested that the pairs were not significantly different. Afterward, the independent factors were used to create the landslide susceptibility maps using the ArcGIS 9.3 platform.

The W_c values of the conditioning factors are shown in Table 2. Although the training datasets are different, the W_c values of the relationship between LSI and land use/cover are higher in woodland areas than other land use areas except for the bamboo area. The bamboo area has the highest W_c values except when choosing the RL sampling strategy where the grassland has the highest weight contrast. The W_c values are also high in the areas where the elevations range from 250–400 m; when the elevations are higher than 400 m, the probabilities of LS decrease. Relationships between curvature and landslide occurrence indicate that landslides generally do not occur near areas where the curvature has values smaller than −1.5 or larger than 2.5. The W_c values of distance to faults between 800 m and 2000 m are positive, revealing a high correlation with LS. Also, the flow directions of E, SE and S directions have high probabilities of LS. The W_c values are larger for TWI and range from 0.5–2, which indicates a high positive spatial correlation. The WOE results demonstrate that areas with slopes between 10–20° have high probabilities of landslide occurrence. W_c values are also high in the areas where the distance to stream is smaller than 400 m, indicating high probabilities of LS. Relationships between distance to highways and landslide occurrence indicate that landslides generally occurred near the highways, with distances smaller than 1500 m, which was similar to the FR model results. With different sampling strategies, the roles of geologic condition are different. The Wc values of geology are higher in J2-3ac, and K2vf has high probabilities of LS using the RD and RL sampling strategies. When the TD sampling strategy was applied, the Wc value of J2-3ac indicates a highly negative spatial correlation with LS. Those results also indicate the importance of geologic conditions for landslide susceptibility mapping. The WOE models are used to create the LS maps shown in Figure 5.

4.4. Logistic Regression (LR)

The logistic regression (LR) model is a commonly used mathematical method to establish the relationship between conditioning factors and landslides (Bai et al., 2010; Das et al., 2010; Oh et al., 2010). Some studies have compared the logistic regression model with other methods and have found logistic regression to be the most accurate of these techniques (Bui et al., 2012; Xu et al., 2012). Therefore, a forward stepwise logistic-regression model is applied to create landslide-susceptibility maps. The predicted values range from 0 to 1, and can be defined by the following formulas:

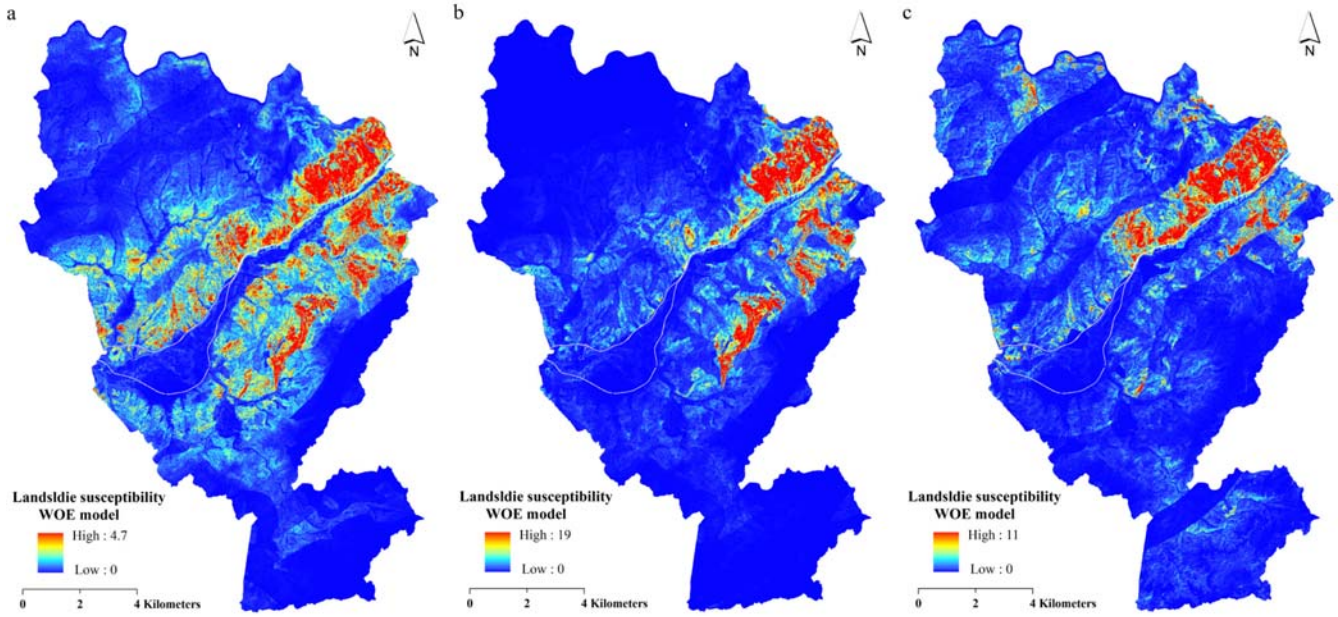

Fig. 5. Landslide susceptibility maps using WOE model. (a) RD sampling strategy; (b) RL sampling strategy; (c) TD sampling strategy.

$$y = b_0 + b_1x_1 + b_2x_2 + \ldots + b_nx_n\,, \tag{7}$$

$$p = e^y/(1+e^y)\,, \tag{8}$$

where y is the linear logistic model, b_0 is the intercept of the model, n is the number of landslide-controlling factors, b is the weight of each factor, x represents the landslide conditioning factors and P is the probability of landslide occurrence (landslide susceptibility index).

Two important parameters, tolerance (TOL) and the variance inflation factor (VIF), were used to determine the colinearities between independent variables. If TOL < 0.4 and VIF > 2, those parameters were not selected in the logistic regression models (Bui et al., 2012). In this study, there are no high correlations among the dependent variables. The training datasets were then used in the SPSS software to model the relationship between the probability of landslide occurrence and the conditioning factors. The last category was assigned as the reference category for each categorical variable. The spatial relationship between landslide occurrence and conditioning factors was assessed using the LR model with different training datasets.

Table 3 demonstrates that the results of the models had statistical significance and that the independent variables could account for the variance in the dependent variables in the models by using Cox & Snell R^2 values, which range from 0.36 to 0.43, and Nagelkerke R^2 values ranging from 0.49 to 0.57. Table 3 also reveals that the sampling strategies have no important impact on model performance because the Cox & Snell R^2 and Nagelkerke R^2 values are very close to each other.

The coefficients of the LR model are shown in Figure 6. From Figure 6, the statistical relationship between conditioning factors and landslide occurrence can be understood. It is found that LR coefficients had generally positive correlations with TWI with different training datasets. All of the coefficients of the TWI classes are positive. This means that TWI is positively related to the occurrence of a landslide. We also determined that the importance of each landslide conditioning factor for landslide occurrence is very different with different training datasets. The highest LR coefficients of elevation range from 250–400 m, except when choosing the TD sampling strategy, where elevation has no influence on a landslide occurrence. LR coefficients generally have negative correlations with distance to stream, except when using the TD sampling strategy, where this factor plays no role in the occurrence of landslides. Relationships between distance to highways and landslide occurrence indicate that landslides generally occurred near highways, with distances

Table 3. Statistics and accuracy of the logistic regression models

	Hosmer and Lemeshow			–2 Log likelihood	Cox & Snell R Square	Nagelkerke R Square	Predicted accuracy
	Chi-square	df	Sig.				
$LR_{(RD)}$	29.997	8	0.00	23058.540	0.428	0.572	0.80
$LR_{(TD)}$	118.735	8	0.00	24963.426	0.360	0.492	0.79
$LR_{(RL)}$	120.044	8	0.00	24675.432a	0.404	0.544	0.81

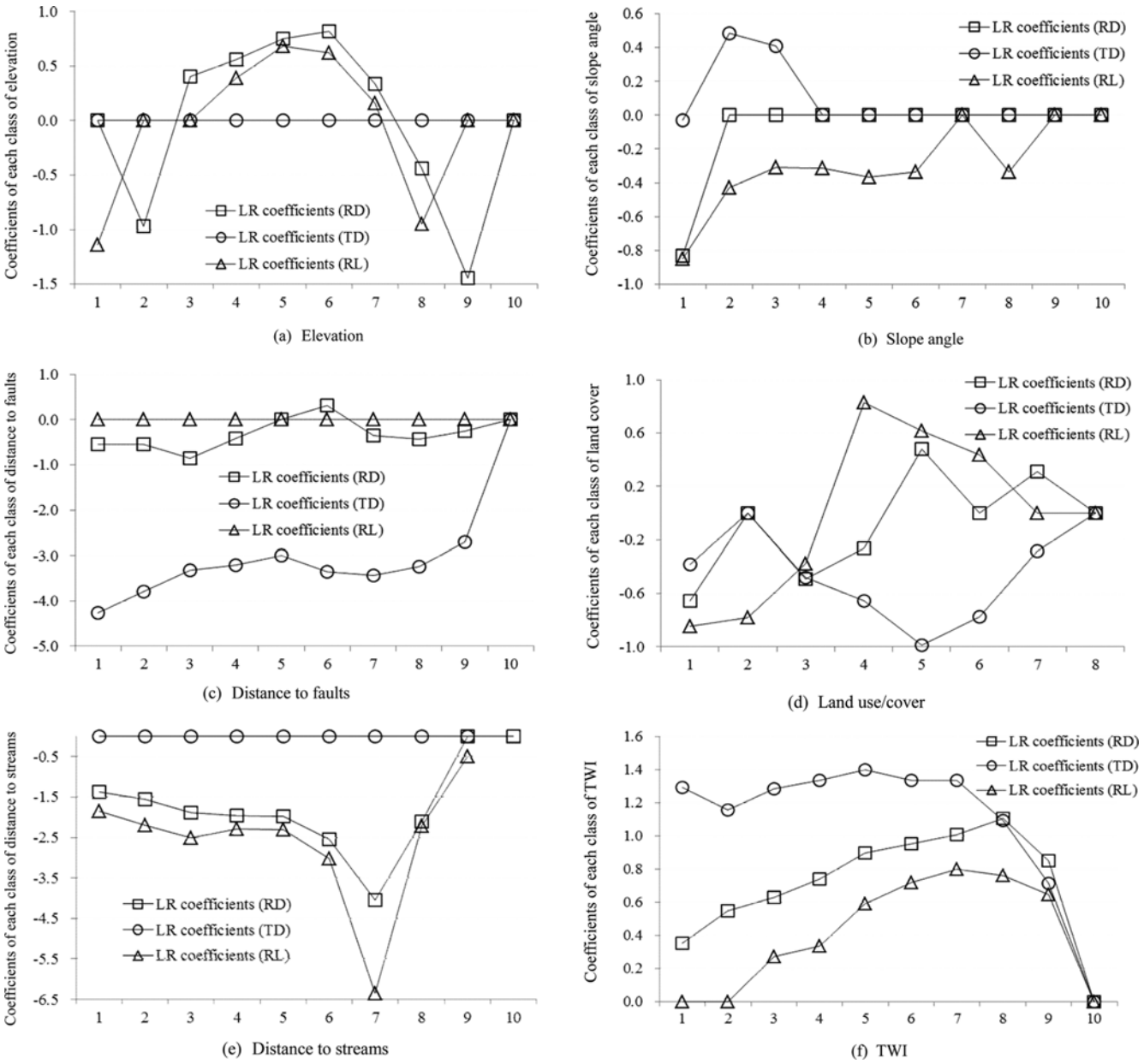

Fig. 6. LR coefficients for the study area. (a) Elevation; (b) Slope angle; (c) Distance to faults; (d) landuse/cover; (e) Distance to streams; (f) TWI; (g) Flow direction; (h) Distance to highways; (i) Curvature; (j) Geologic unit. The horizontal axis is corresponding to the ID number in Table 2.

smaller than 1500 m, except when choosing the RL sampling strategy. Figure 6 shows that LR coefficients have strongly negative correlations with distance to faults using the TD sampling strategy, but when we select the RL sampling datasets, the correlation between LR and distance to faults vanishes. From Figure 6, the coefficients demonstrate that slopes between 5–15° have positive correlations with landslide occurrence using the TD sampling strategy; otherwise, the slope has a negative correlation with LS. The coefficients for curvature are negative, revealing high correlations with LS. The value of flow direction equal to 2 has a positive correlation with LS using the RD sampling strategy. The other coefficients of flow direction indicate negative correlations with landslide occurrence. The relationship between LS and land use/cover are complicated by the use of different sampling strategies. The grassland area has the highest positive weight using the RD sampling strategy, while the grassland has a negative correlation with LS using TD sampling strategy. Using RL, the forest has high probabilities of LS with positive correlations, and otherwise have negative correlations with landslide occurrence. The coefficient values of geology are higher in J2-3ac, and K2vf exhibits high probabilities of LS using both the RD

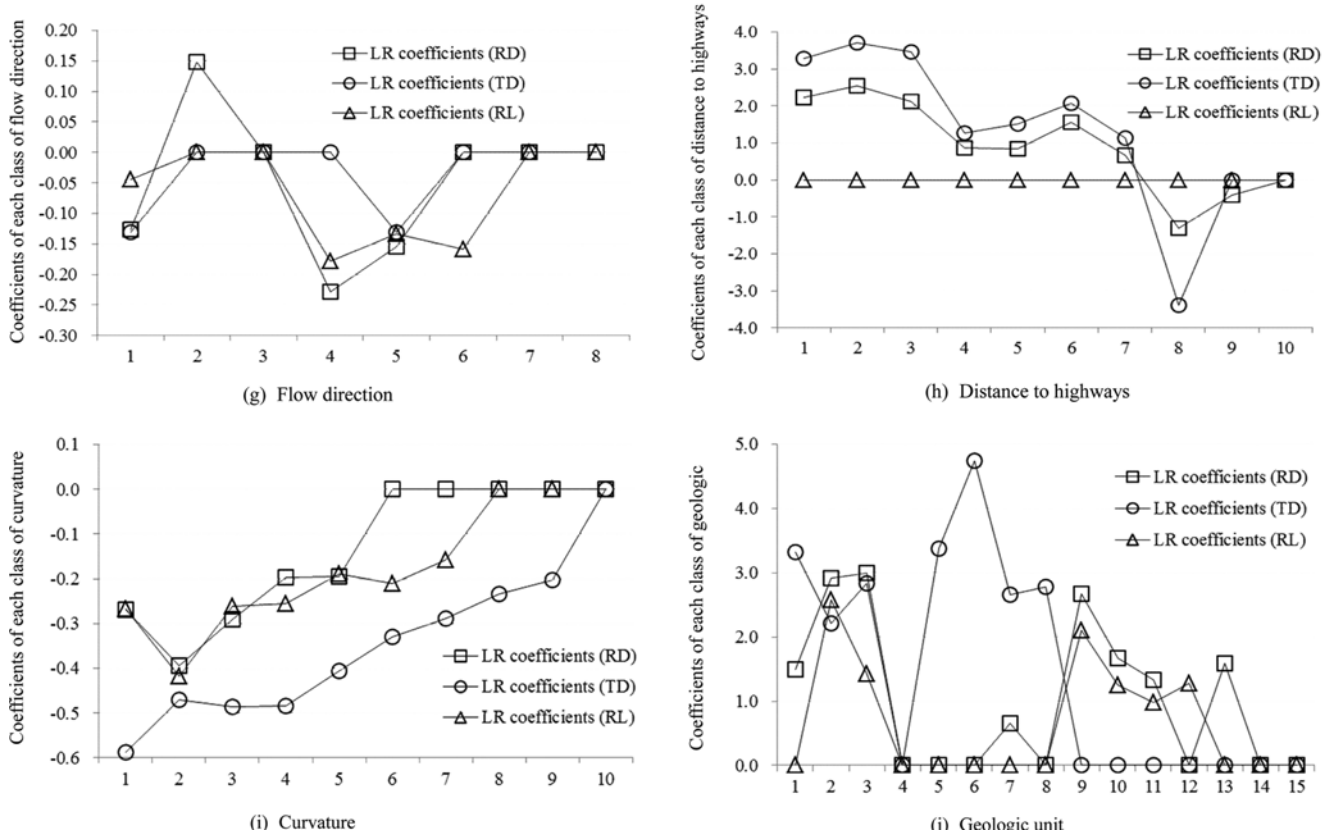

Fig. 6. (continued).

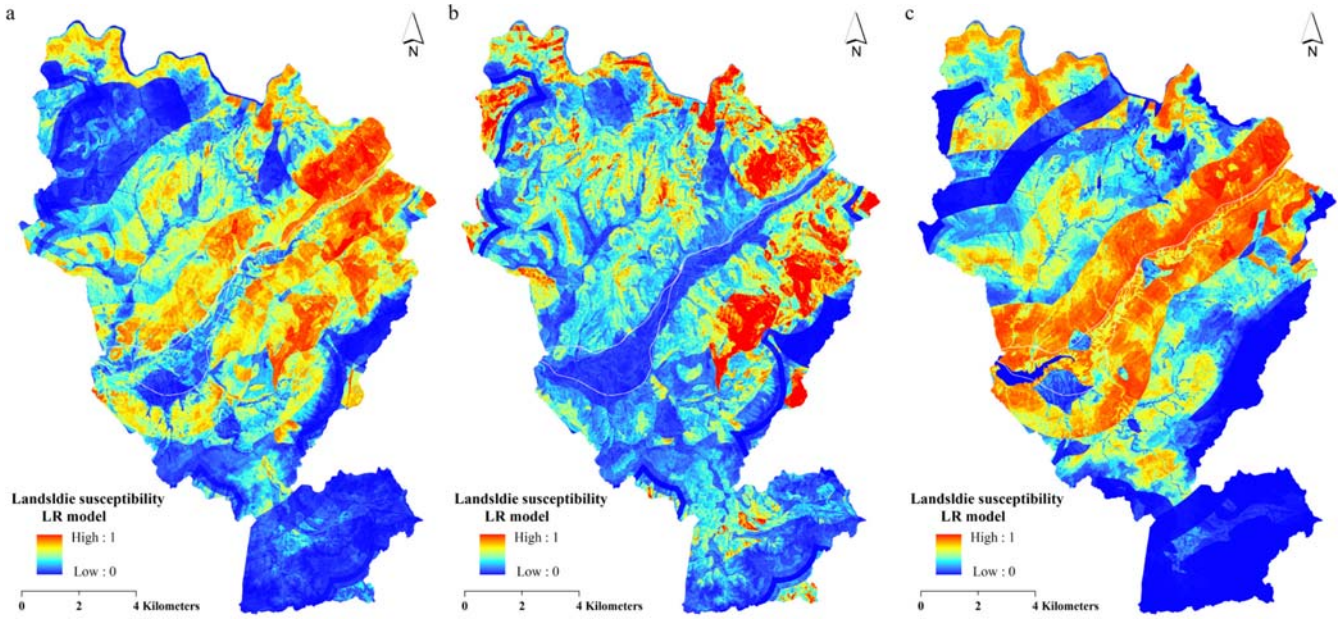

Fig. 7. Landslide susceptibility maps using LR model. (a) RD sampling strategy; (b) RL sampling strategy; (c) TD sampling strategy.

and RL sampling strategies. When the TD sampling strategy was applied, the coefficient of K2gd indicates a high spatial correlation with LS. The above analyses indicate that the sampling strategy may affect the model performances. Based on formulas 7 and 8, the LS values were calculated using the GIS platform and the factors overlay technology. The LS maps created by LR are shown in Figure 7.

4.5. Decision Tree (DT)

The decision tree model is a technique using tree structures for finding and describing structural patterns in data, and does not require the relationships between all of the input variables and an objective variable in advance (Saito et al., 2009). The objective of the DT model is to build the decision rules that can be used to predicate the relations between the independent variables and an objective variable (Pradhan, 2013). Generally, a decision tree structure has three parts from top to bottom, such as a root node, a set of internal nodes, and a set of terminal nodes (leaves). The processing is carried out by moving down the tree until the terminal node is reached (Saito et al., 2009). There are four major algorithms for construction of decision tree models, including classification and regression tree (CART), chi-square automatic interaction detector decision tree (CHAID), ID3 and C4.5 (Pradhan, 2013). In this study, CART was selected as the decision tree model because of the performance efficiency (Felicisimo et al., 2013). The implementation of CART was carried out with SPM software with all of the training datasets (Salford Systems, http://www.salfordsystems.com/). The CART creates complex tree constructions that are later pruned back to avoid overfitting. In this study, a 10-fold cross-validation was also adopted to evaluate the robustness of the decision-tree model, along with optimizing the decision-tree size (Saito et al., 2009). Therefore, the numbers of the terminal nodes are less than 21 nodes, and some less important factors were excluded. Figure 8 shows the effect of each landslide conditioning factor with different training datasets for the DT model. The lithological formations in the study area have the most important influence on landslide occurrence. When the TD sampling strategy is chosen for model construction, the distance to highway and distance to fault values play a key role in model performance. The elevation factor is very efficient for landslide occurrence when the RL sampling strategy is used for training. Distance to stream is more important when using the RL sampling strategy. Landuse/landcover is also a key factor for landslide susceptibility mapping. The LS maps created by DT can be found in Figure 9.

4.6. Artificial Neural Network (ANN)

A neural network may be used as a direct substitute for auto correlation, multivariable regression, linear regression, trigonometric, and other statistical analysis and techniques (Yilmaz, 2010). An artificial neural network model (ANN) has a capacity to imitate the neural system of human brains (Xu et al., 2012). Therefore, it can extract patterns and detect trends that are too complex to be noticed by other techniques (Yilmaz, 2009). The ANN model acts as an expert to detect important predictive patterns that are not obvious to a non-expert. Compared with other statistical models, an ANN model has the ability to cope with imprecise and fuzzy data, so they can handle continuous, category and binary data without violating any assumptions (Yilmaz, 2009). Therefore, it is considered an efficient approach for landslide susceptibility analysis.

Among many types of ANN models, the back-propagation (BP) training algorithm is the most frequently and instructively used neural network model, also it is accepted as one of the most useful neural networks for landslide susceptibility prediction and decision making (Yilmaz, 2010; Pradhan and Lee, 2010a, 2010b). In this study, the BP algorithm is used.

The purpose of ANN is to build a model of data-generating processes so the network can generalize and predict outputs from inputs (Pradhan and Lee, 2010b). The BP algorithm is

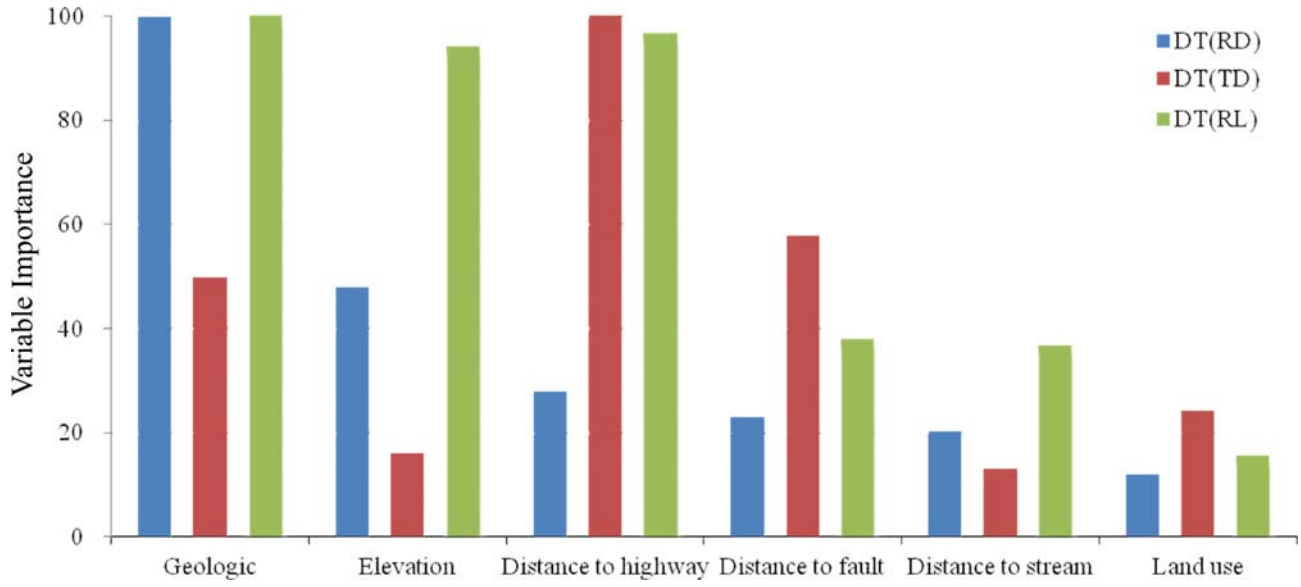

Fig. 8. Parameter importance map obtained from DT model. The horizontal axis is the factor importance.

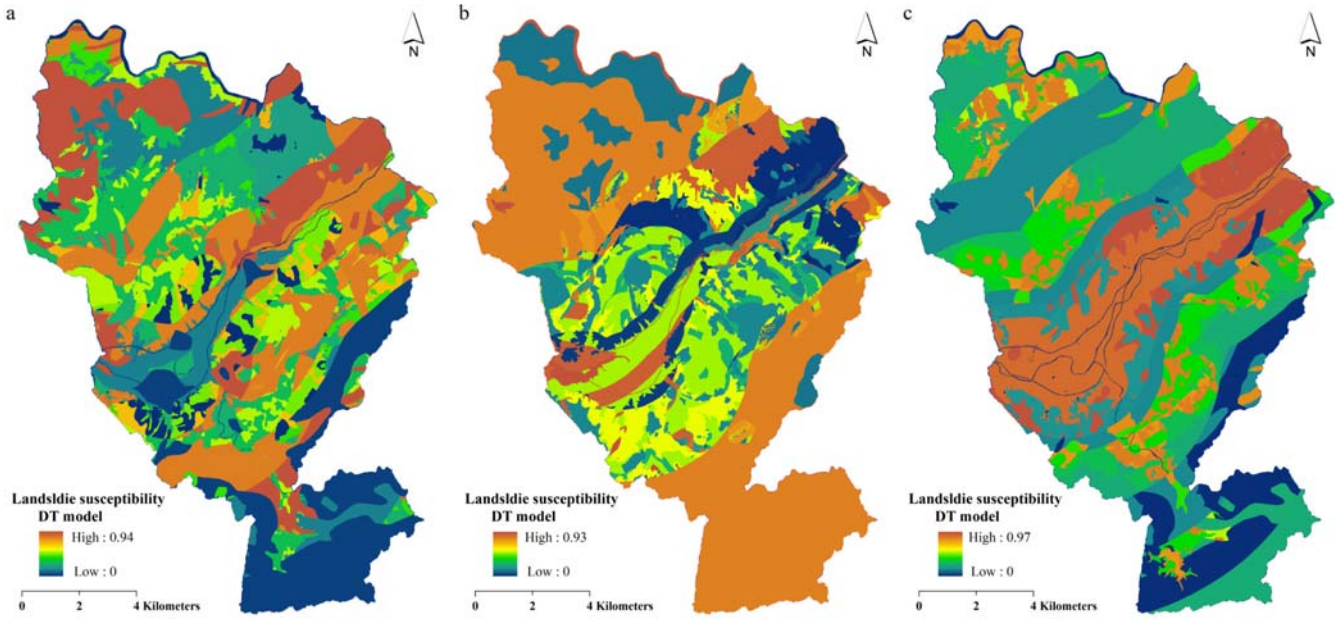

Fig. 9. Landslide susceptibility maps using DT model. (a) RD sampling strategy; (b) RL sampling strategy; (c) TD sampling strategy.

a multi-layer neural network, which has an input layer, several hidden layers and an output layer (Pradhan and Lee, 2010b). The hidden layer neurons process the inputs through a series of calculations, such as multiplying each input by a corresponding weight, summing the product, and subsequently processing the sum with a nonlinear transfer function to produce a result (Pradhan and Lee, 2010b; Xu et al., 2012). At the end of the training process, the artificial neural network creates a model that has the ability to predict a target value from a given input value (Pradhan and Lee, 2010b). The architecture and detailed algorithm of neural networks can be found in the literature (Yilmaz, 2009; Yilmaz, 2010; Pradhan and Lee, 2010b).

The data used in the ANN model should be partitioned into at least two subsets, such as training and test datasets. The training dataset is used in the training stage of the model development to update the weights of the network, and then the test dataset, which is different from the training dataset, is applied to evaluate the network performance and confirm its accuracy (Pradhan and Lee, 2010b). There are no exact mathematical rules to determine the required minimum size these subsets (Nefeslioglu et al., 2008). Therefore, three groups

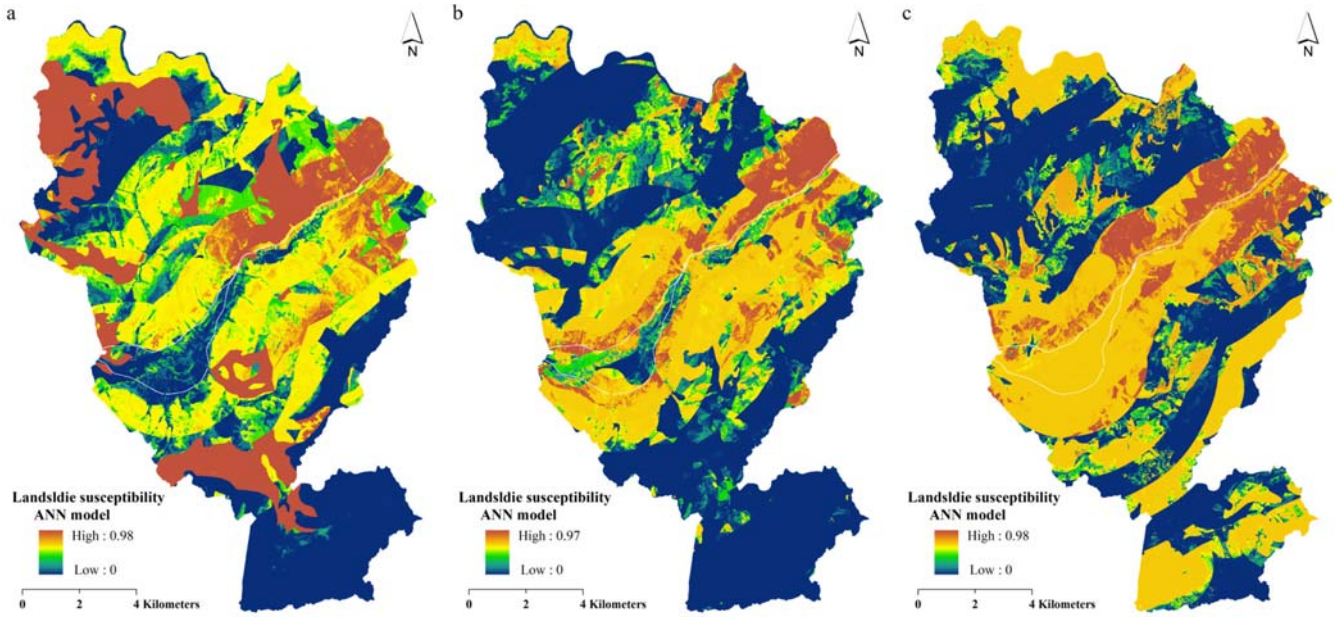

Fig. 10. Landslide susceptibility maps using ANN model. (a) RD sampling strategy; (b) RL sampling strategy; (c) TD sampling strategy.

of training and test datasets (including RD, TD and RL samplings) are used in this study.

The ENVI software package was used for training and testing the ANN model. A three layer feed-forward network that consists of an input layer, one hidden layer, and one output layer was used as a network structure (Xu et al., 2012). Three groups of training datasets were selected in the study, and the factors were adjusted using the same parameters of the ANN model as follows (Xu et al., 2012);

Activation function: Logistic;
Training threshold contribution: 0.9;
Training rate: 0.2;
Training momentum factors: 0.9;
Training root square error exit criteria: 0.1;
Number of hidden layers: 1;
Number of training iterations: 1000;

As in many other network training methods, models and parameters were used to reach minimum Root mean square (RMS) values (Yilmaz, 2009). In this study, the RMS values of training and testing were set as 0.01 for the ANN structure. After the network goal was reached, the study area was fed into the network to estimate the landslide susceptibility (Yilmaz, 2009). The sets of the landslide susceptibility indexes of each grid were calculated, and landslide susceptibility maps are shown in Figure 10.

5. RESULT AND COMPARISON

There are many classification methods available such as natural breaks, equal intervals and standard deviations (Ayalew and Yamagishi, 2005; Pradhan, 2013). In this paper, the landslide susceptibility-index maps were divided into four classes by the natural breaks method under the ArcGIS platform. The accuracy of the landslide susceptibility maps were evaluated by calculating the relative operative characteristic (ROC) and the percentage of observed-landslide points in various susceptibility categories using three different test datasets (Nandi and Shakoor, 2010). The area under the ROC curve (AUC) represents the quality of the probabilistic model (its ability to predict the occurrence or non-occurrence of an event) (Yesilnacar and Topal, 2005). The value of AUC ranges from 0.5 to 1. An AUC value close to 1 indicates high accuracy, and an AUC value close to 0.5 indicates inaccuracy (Fawcett, 2006).

Figure 11 shows the percentage of observed-landslide points in various susceptibility categories using three different test datasets. From Figure 11a, more than 80% of observed landslides are found in high and very high susceptibility classes for the ANN and DT models, whereas the FR and LR models indicate that approximately 70% of the landslides are concentrated in the high and very high susceptibility classes. Over 48% and 44% of the landslides occur in areas with very high susceptibility classes based on ANN, and LR, respectively. The proportion of landslides that had high to very high susceptibility was 90.3% based on ANN model, which was higher than for the DT (83%) and LR (72%) models. The WOE model had the lowest value, which was only 22.4%. Additionally, using the RL sampling strategy (Fig. 11b), only 61% of the landslides were concentrated in the high and very high categories of the DT model, which was the highest. For the ANN, LR and FR models, approximately 57.7%, 22.3% and 30.1% of the landslides were in the high and very high categories. WOE has the highest percentage of landslide bodies in the very low category, approximately 61%, which is an unacceptable result. Figure 11c shows that the very high category contains 58.1% and 42.5% of the landslide bodies using the LR and DT models, respectively. The highest proportion of landslides appearing from high to very high susceptibility is 86.3%, based on the LR model. However, the DT and ANN models contain 58.1% and 42.5%, respectively, of the landslide points falling in the high and very high classes. Over 30% of the landslide points concentrate in the low and very low categories, which is an unacceptable result. Comparing the results from all of the models, we determine that better results could be obtained by using the LR and DT models with a higher percentage of landslide points concentrated in high and very high classes using a different sampling strategy.

Some landslide susceptibility indexes obtained from mathematical models are outside of the range of 0 to 1. The following equation (Eq. 9) was applied to transform the landslide susceptibility index to values between 0 and 1, and then the ROC curve was used to assess the quality of the landslide susceptibility maps;

$$L_i = \frac{L_i - L_{\min}}{L_{\max} - L_{\min}}, \tag{9}$$

where, L_i is the normalized value of the landslide susceptibility index, L_{min} is the minimum value of L_i, and L_{max} is the maximum value of L_i.

When the ROC curves of these five mathematical methods were considered together, their overall performance could be identified (Fig. 12). Figure 12 shows the AUC values of test landslide points by different mathematical models. According to the obtained AUC, LR has slightly higher prediction performance (0.787) than WOE (0.777), FR (0.776), DT (0.744) and ANN (0.737) using the random (RD) sampling strategy. Additionally, LR also provides a higher prediction performance (0.865) than FR (0.772) and DT (0.724) using the TD sampling strategy. In contrast, when the LR sampling strategy is applied, DT has the highest AUC value (0.704). The results may be observed because the random (RD) sampling strategy covers all of the spatial distribution characteristics of landslides and makes the five mathematical models slightly more successful than the TD and RL sampling strategies which only partially cover landslide spatial distribution characteristics. The WOE model exhibits poor calculation results for all of the sampling strategies. This may be observed because in the WOE model, the relationships between sampling points and con-

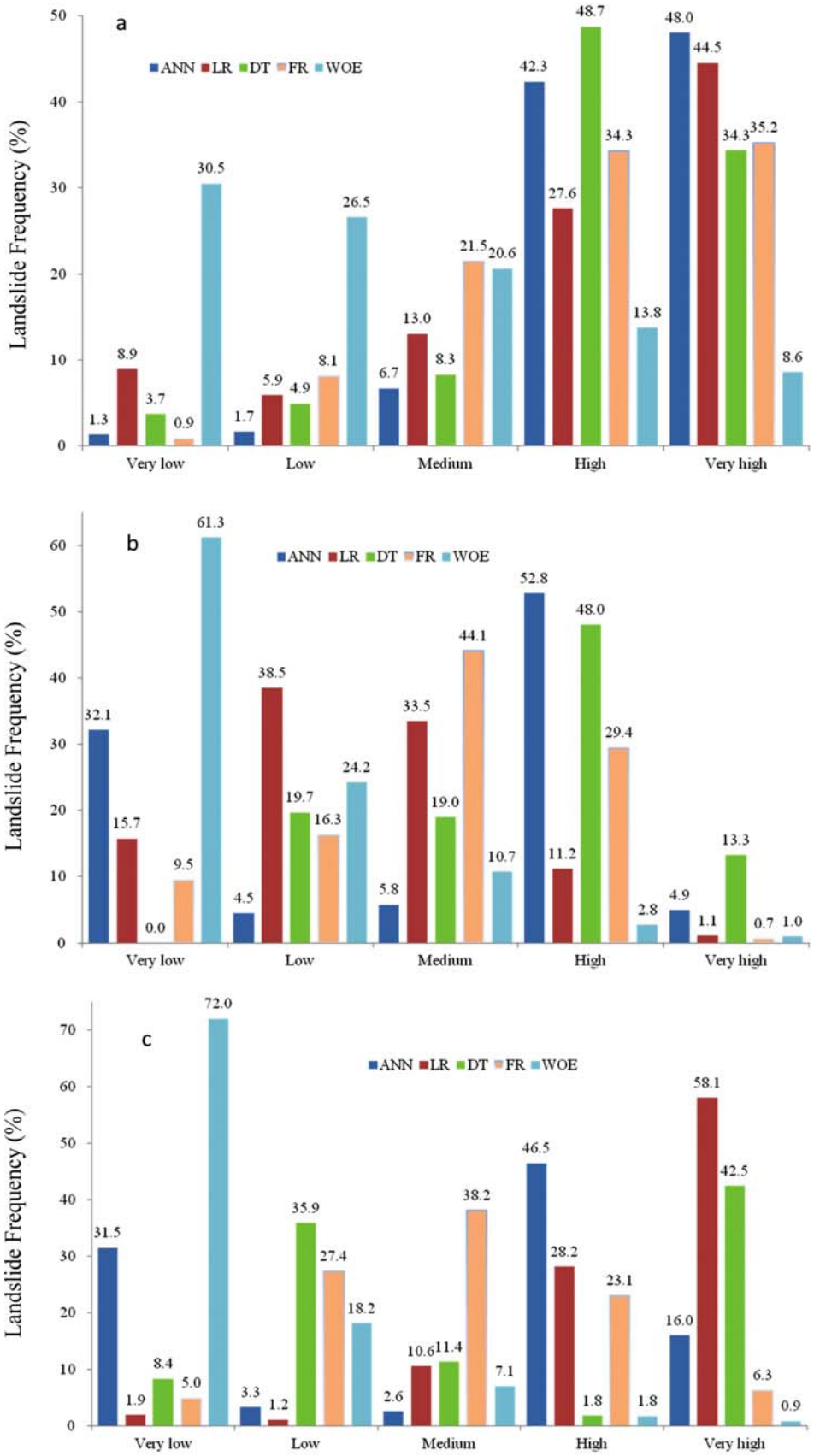

Fig. 11. Percentages of observed landslides falling into different susceptibility categories using ANN, FR, LR, DT and WOE using different sampling strategies. (a) RD sampling strategy; (b) RL sampling strategy; (c) TD sampling strategy.

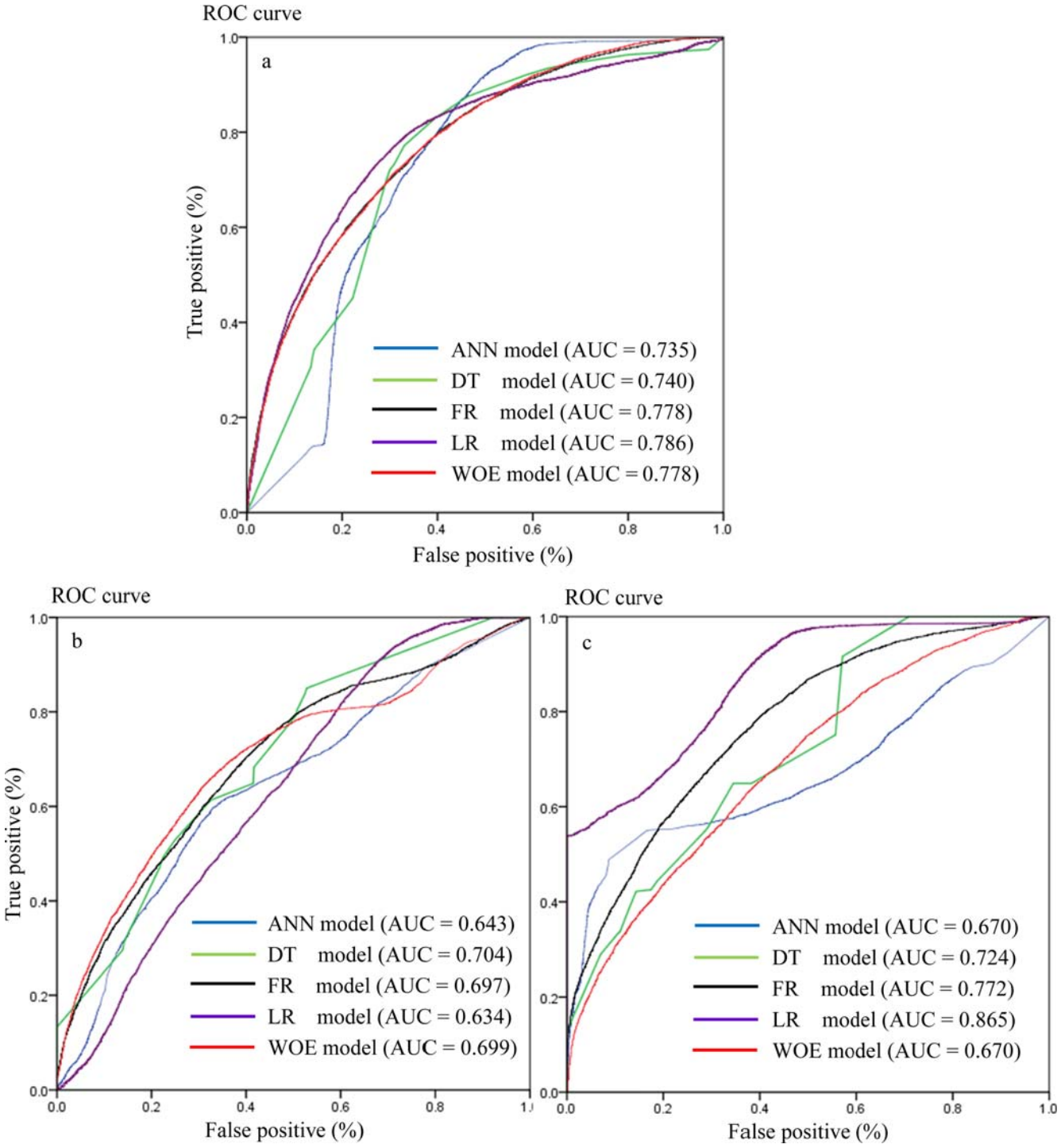

Fig. 12. ROC curves evaluation of the five models. (a) RD sampling strategy; (b) RL sampling strategy; (c) TD sampling strategy.

ditioning factors are poorly related, and fewer connections make the WOE performance poorer than other models. Therefore, one can conclude here that the selection of mathematical model has an impact on the overall prediction performance of a landslide susceptibility analysis. The LR model has the highest AUC value when using the TD sampling strategy, which may be due to the following reasons. First of all, most of the large scale unstable slopes were along the two highways (see Fig. 1). The large number of training points from the upside of a highway makes the data richer, and the enrichment makes the LR model more accurate than other methods. Another reason may be the fortuitous of the calculation result. When

using the RL sampling strategy, the LR model has a high percentage of landslide points falling in the low category because this sampling strategy ignores the true distribution pattern of the landslides. This is the reason why sampling strategy plays a key role in landslide susceptibility mapping. Apart from the above result, it is clear that DT methods have performed reasonably well, with AUC > 0.7 prediction performance using the various sampling strategies.

From the above analysis, the various datasets may affect the landslide susceptibility model performance. That is the main topic in the paper. When the purpose of this study is considered, local governments should first consider the landslide distribution pattern of the study area, choose the suitable sampling strategy, and then select the proper methods to produce reliable landslide susceptibility maps.

6. DISCUSSION AND CONCLUSIONS

In this paper, five mathematical models, including the ANN, FR, DT, LR and WOE methods, with three sampling strategies are used to analyze landslide susceptibility and create landslide susceptibility maps that are useful to local authorities. According to the results, the LR and DT models achieved more efficient model performance with higher percentages of test landslide points falling in high and very high classes and a steady AUC value. The ANN, FR, DT, LR and WOE methods should be used and assessed carefully by a landslide expert or a geological engineer because these powerful methods are easily affected by the training and test landslide datasets. In this study, the results obtained from DT show steady prediction power with an AUC value larger than 0.7. Additionally, the results with the RD (random) sampling strategy provided more reliable model performance with a higher percentage of test landslide points falling in high and very high classes and with high AUC values (AUC > 0.7). However, it is noted that the performance of landslide susceptibility maps depends not only on the mathematical model used but also on the selected training and test dataset. For this reason, if the proper landslide points are selected by field observation, the performance of the landslide susceptibility results produced by the ANN, FR, DT, LR and WOE methods may increase. To some extent, the landslide susceptibility maps could not provide more detailed information on the landslide-prone areas at the medium scale for Mizunami City, but the maps would provide the local authorities with the spatial distribution trend of a landslide that may occur in the future. Additionally, the landslide mechanism in the study area is very complicated. There is still an indispensable need for further investigation of landslide mechanisms in Mizunami City.

ACKNOWLEDGMENTS: This research is supported by High Academic Talent Foundation Nanjing Forestry University (Grant No. GXL2014037), National Basic Research Program of China (Grant No. 31200534), Priority Academic Program Development of Jiangsu High Education Institutions (PAPD) and Gifu University. The author would like to thank two anonymous reviewers for their constructive comments and suggestions which significantly improved the quality of this paper.

REFERENCES

Ayalew, L. and Yamagishi, H., 2005, The application of GIS-based logistic regression for landslide susceptibility mapping in the Kakudayahiko Mountains, Central Japan. Geomorphology, 65, 15–31.

Althuwaynee, O.F., Pradhan, B., Park, H.J., and Lee, J.H., 2014, A novel ensemble bivariate statistical evidential belief function with knowledge-based analytical hierarchy process and multivariate statistical logistic regression for landslide susceptibility mapping. Cantena, 114, 21–36. doi:10.1016/j.catena.2013.10.011

Bai, S.B., Wang, J., Guo, N.L., Zhou, P.G., Hou, S.S., and Xu, S.N., 2010, GIS-based logistic regression for landslide susceptibility mapping of the Zhongxian segment in the Three Gorgesarea, China. Geomorphology, 115, 23–31.

Bui, D.T., Pradhan, B., Lorfman, O., Revhaug, I., and Dick, O.B, 2012, Landslide susceptibility assessment in the Hoa Binh province of Vietnam: A comparison of the Levenberg–Marquardt and Bayesian regularized neural networks. Geomorphology, 171–172, 12–29. doi:10.1016/j.geomorph.2012.04.023

Conforti, M., Pascale, S., Robustelli, G., and Sdao, F., 2014, Evaluation of prediction capability of the artificial neural networks for mapping landslide susceptibility in the Turbolo River catchment (northern Calabria, Italy). Cantena, 113, 236–250. doi:10.1016/j.catena.2013.08.006

Das, I., Sahoo, S., Van Westen, C., Stein, A., and Hack, R., 2010, Landslide susceptibility assessment using logistic regression and its comparison with a rock mass classification system, along a road section in the northern Himalayas (India). Geomorphology, 114, 627–637.

Fawcett, T., 2006, An introduction to ROC analysis. Pattern Recognition Letters, 27, 861–874

Felicisimo, A., Cuartero, A., Remondo, J., and Quiros, E., 2013, Mapping landslide susceptibility with logistic regression, multiple adaptive regression splines, classification and regression trees, and maximum entropy methods: a comparative study. Landslides, 10, 175–189.

Mittal, S.K., Singh, M., Kapur, P., Sharma, B.K., and Shamshi, M.A., 2008, Design and development of instrument network for landslide monitoring, an issue an early warning. Journal of Scientific & Industrial research, 67, 361–365.

Nandi, A. and Shakoor, A., 2010, A GIS-based landslide susceptibility evaluation using bivariate and multivariate statistical analyses. Engineering Geology, 110, 11–20.

Nefeslioglu, H.A., Gokceoglu, C., and Sonmez, H., 2008, An assessment on the use of logistic regression and artificial neural networks with different sampling strategies for the preparation of landslide susceptibility maps. Engineering Geology, 97, 171–191.

Neuhauser, B., Damm, B., and Terhorst, B., 2011, GIS-based assessment of landslide susceptibility on the base of the weights of evidence model. Landslides, 9, 511–528.

Nourani, V., Pradhan, B., Ghaffari, H., and Sharifi, S.S., 2014, Landslide susceptibility mapping at Zonouz Plain, Iran using genetic programming and comparison with frequency ratio, logistic regression, and artificial neural network models. Natural Hazards, 71, 523–547.

Lee, S. and Talib, J.A., 2005, Probabilistic landslide susceptibility and factor effect analysis. Environmental Geology, 47, 982–990.

Oh, H.J., Lee, S., and Soedradjat, G., 2010, Quantitative landslide susceptibility mapping at Pemalang area, Indonesia. Environmental Earth Sciences, 60, 1317–1328.

Ozdemir, A. and Altural, T., 2013, A comparative study of frequency ratio, weights of evidence and logistic regression methods for landslide susceptibility mapping: Sultan Mountains, SW Turkey. Journal of Asian Earth Sciences, 64, 180–197.

Poudyal, C.P., Chang, C., Oh, H.J., and Lee, S., 2010, Landslide susceptibility maps comparing frequency ratio and artificial neural networks: a case study from the Nepal Himalaya. Environmental Earth Sciences, 61, 1049–1064.

Pradhan, B., 2010a, Landslide susceptibility mapping of a catchment area using frequency ratio, fuzzy logic and multivariate logistic regression approaches. Journal of the Indian Society of Remote Sensing, 38, 301–320.

Pradhan, B., 2010b, Remote sensing and GIS-based landslide hazard analysis and cross validation using multivariate logistic regression model on three test areas in Malaysia. Advances in Space Research, 45, 1244–1256.

Pradhan, B., 2013, A comparative study on the predictive ability of the decision tree, support vector machine and neuro-fuzzy models in landslide susceptibility mapping using GIS. Computers & Geosciences, 51, 350–365.

Pradhan, B. and Lee, S., 2010a, Delineation of landslide hazard areas on Penang Island, Malaysia, by using frequency ratio, logistic regression, and artificial neural network models. Environmental Earth Sciences, 60, 1037–1054.

Pradhan, B. and Lee, S., 2010b, Landslide susceptibility assessment and factor effect analysis: back-propagation artificial neural networks and their comparison with frequency ratio and bivariate logistic regression modelling. Environmental Modelling & Software, 25, 747–759.

Pradhan, B., Lee, S., and Buchroithner, M.F., 2010, A GIS-based back-propagation neural network model and its cross application and validation for landslide susceptibility analyses. Computers, Environment and Urban Systems, 34, 216–235.

Regmi, N.R., Giardino, J.R., and Vitek, J.D., 2010a, Assessing susceptibility to landslide: Using models to understand observed changes in slopes. Geomorphology, 122, 25–38.

Regmi, N.R., Giardino, J.R., and Vitek, J.D., 2010b, Modeling susceptibility to landslides using the weight of evidence approach: western Colorado, USA. Geomorphology, 115, 172–187.

Saito, H., Nakayama, D., and Matsuyama, H., 2009, Comparison of landslide susceptibility based on a decision tree model and actual landslide occurrence: The Akaishi Mountains, Japan. Geomorphology, 109, 108–121.

Shahabi, H., Hhezri, S., Ahmhad, B.B., and Hashim, M., 2014, Landslide susceptibility mapping at central Zab basin, Iran: A comparison between analytical hierarchy process, frequency ratio and logistic regression models. Catena, 115, 55–70.

Vahidnia, M.H., Alesheikh, A.A., Alimohammadi, A., and Hosseinali, F., 2010, A GIS-based neuro-fuzzy procedure for integrating knowledge and data in landslide susceptibility mapping. Computers & Geosciences, 36, 1101–1114.

Van Westen, C.J., Rengers, N., and Soeters, R., 2003, Use of geomorphological information in indirect landslide susceptibility assessment. Natural Hazards, 30, 399–419.

Varnes, D.J., 1978, Slope movements: types and processes. In: Schuster, R.L. and Krizek, R.J. (eds.), Landslide analysis and control. National Academy of Sciences, Transportation Research Board Special Report 176, Washington, 11–33.

Wang, L.J., Sawada, K., and Moriguchi, S., 2013, Landslide susceptibility analysis with logistic regression model based on FCM sampling strategy. Computers & Geosciences, 57, 81–92.

Xu, C., Xu, X., Dai, F., and Saraf, A., 2012, Comparison of different models for susceptibility mapping of earthquake triggered landslides related with the 2008 Wenchuan earthquake in China. Computers & Geosciences, 46, 317–329.

Yalcin, A., 2008, GIS-based landslide susceptibility mapping using analytical hierarchy process and bivariate statistic in Ardesen (Turkey): comparisons of result and confirmations. Catena, 72, 1–12.

Yalcin, A., Reis, S., Aydinoglu, A.C., and Yomralioglu, T., 2011, A GIS-based comparative study of frequency ratio, analytical hierarchy process, bivariate statistics and logistics regression methods for landslide susceptibility mapping in Trabzon, NE Turkey. Catena, 85, 274–287.

Yeon, Y.-K., Han, J.-G., and Ryu, K.H., 2010, Landslide susceptibility mapping in Injae, Korea, using a decision tree. Engineering Geology, 116, 274–283.

Yesilnacar, E. and Topal, T., 2005, Landslide susceptibility mapping: a comparison of logistic regression and neural networks methods in a medium scale study, Hendek region (Turkey). Engineering Geology, 79, 251–266.

Yilmaz, I., 2009, Landslide susceptibility mapping using frequency ratio, logistic regression, artificial neural networks and their comparison: a case study from Kat landslides (Tokat-Turkey). Computers & Geosciences, 35, 1125–1138.

Yilmaz, I., 2010, Comparison of landslide susceptibility mapping methodologies for Koyulhisar, Turkey: conditional probability, logistic regression, artificial neural networks, and support vector machine. Environmental Earth Sciences, 61, 821–836.

Manuscript received August 18, 2014
Manuscript accepted April 21, 2015